Journal of Materials Chemistry C

ROYAL SOCIETY OF CHEMISTRY

PAPER

View Article Online
View Journal | View Issue

Cite this: J. Mater. Chem. C, 2022, 10, 13797

Modulation of the intramolecular hydrogen bonding and push–pull electron effects toward realizing highly efficient organic room temperature phosphorescence†

Guoyu Jiang, ‡[a] Qiyao Li,‡[b] Anqi Lv,‡[c] Lingxiu Liu,[a] Jianye Gong,[a] Huili Ma, *[c] Jianguo Wang *[a] and Ben Zhong Tang *[b]

The exploitation of ultralong organic room temperature phosphorescence (UORTP) materials lags far behind the need because of the lack of general design strategies. Here we proposed a facile design strategy based on the structural control of intramolecular hydrogen bonding (IHB) and push–pull electron effects (PPEEs) to construct highly efficient UORTP materials. Two series of carbazole derivatives with different IHBs and PPEEs were designed accordingly. By enhancing the IHB interactions of the luminophores, the molecular planarity, intermolecular interactions and packing mode were effectively tuned, facilitating the intermolecular electron coupling. PPEEs, enhanced by introducing heteroatoms and heavy atoms, strengthened the intramolecular charge transfer states, which changed the orbital transition configuration of excited states, thus boosting the intersystem crossing (ISC) and spin–orbit coupling (SOC). Consequently, CzPM and CzPMBr with dual IHBs and the strongest PPEEs exhibited ultralong lifetimes (τ_P) of 1.31 s and 233 ms with the highest phosphorescence quantum yields (Φ_P) of 1.7% and 48.6% in their series, respectively. Theoretical investigations revealed that the high-lying intersystem crossing (HISC) between excited singlet states (S_m, $m > 1$) and triplet states (T_n, $n > 1$) occurred and played a vital role in enhancing the Φ_P values of UORTP materials. Significantly, the SOC matrix elements between S_3 and T_7 ($\xi(S_3,T_7)$) of CzPMBr reached up to 39.95 cm^{-1}. Finally, CzPMBr was successfully used as an anti-counterfeiting ink in calligraphy and painting due to its excellent RTP properties. The design strategy based on the structural control of IHBs and PPEEs will greatly widen the design platform of UORTP materials. Meanwhile, the discovery of the HISC process will also provide a new insight for the design of UORTP materials.

Received 18th March 2022,
Accepted 9th April 2022

DOI: 10.1039/d2tc01093c

rsc.li/materials-c

Introduction

In the last decade, ultralong organic room temperature phosphorescence (UORTP) materials with durations ranging from several seconds to hours have become the focus of scientific research for their potential applications in optoelectronic technologies,[1–6] such as anti-counterfeiting,[7–13] information storage,[14–18] chem/biosensors,[19–21] and bioimaging.[22–28] Being superior in terms of structural versatility, flexibility, processability and biocompatibility, UORTP materials have displayed broader development prospects and are ideal alternatives to inorganic phosphors.[29–32] However, different from the well-developed inorganic counterparts, the design and formulation of pure organic room temperature phosphorescence (RTP) luminophores with bright and long-lived emissions remain to be further explored, due to the inherent problems of organic molecules including inefficient intersystem crossing (ISC)[33] and rapid nonradiative decay rate.[34,35]

According to the first-order perturbation theory, Fermi Golden Rule and Marcus–Levich–Jortner theory, the rate constants of ISC (k_{ISC}) are positively correlated with the spin–orbit coupling (SOC) Hamiltonian and the energy gap (ΔE_{ST}) between the lowest excited singlet (S_1) and triplet states (T_n).[36] Thus, boosting SOC or minimizing the ΔE_{ST} of organic compounds is

[a] College of Chemistry and Chemical Engineering, Inner Mongolia Key Laboratory of Fine Organic Synthesis, Inner Mongolia University, Hohhot 010021, P. R. China. E-mail: wangjg@iccas.ac.cn
[b] School of Science and Engineering, Shenzhen Key Laboratory of Functional Aggregate Materials, The Chinese University of Hong Kong, Shenzhen, Guangdong 518172, P. R. China. E-mail: tangbenz@cuhk.edu.cn
[c] Key Laboratory of Flexible Electronics (KLOFE) & Institute of Advanced Materials (IAM), Nanjing Tech University (NanjingTech), 30 South Puzhu Road, Nanjing 211816, P. R. China. E-mail: iamhlma@njtech.edu.cn

† Electronic supplementary information (ESI) available. CCDC 2085870–2085875. For ESI and crystallographic data in CIF or other electronic format see DOI: https://doi.org/10.1039/d2tc01093c

‡ These authors contributed equally to this work.

an effective approach to obtaining highly efficient UORTP luminophores.[37–40] Common strategies to promote SOC focus on introducing heavy atoms or heteroatomic groups (*e.g.* C=O, N, S, P, *etc.*) with lone pair electrons.[41–43] For example, Kim *et al.* found that the halogen bonding in crystals can activate the heavy atom effect, achieving strong RTP emission with a phosphorescence quantum yield (Φ_P) of up to 55%.[44] Chi and coworkers proposed the intermolecular electronic coupling of n electrons and π units with different excited-state configurations, which can facilitate the ISC process.[43] In terms of reducing ΔE_{ST}, methods including intramolecular donor–acceptor interactions and polymerization have been employed. Tang *et al.* reported an efficient UORTP luminophore with a lifetime of 795 ms and Φ_P of 2.1% by structural isomerism tuning in ΔE_{ST} and the first excited triplet state (T_1) configuration.[45] Zhang *et al.* proposed polymerization-induced energy splitting to create small ΔE_{ST} and thus to promote ISC.[46] On the other hand, suppression of nonradiative deactivation pathways of triplet excitons, such as crystallization,[47,48] polymer–matrix assistance,[49–51] host–guest interactions,[52–58] H-aggregation,[59] intermolecular halogen bonding,[60] ionic crystals,[61] and self-assembly,[62,63] was also found to play critical roles in constructing UORTP luminophores. Although these strategies have largely promoted the development of UORTP materials, most of them are based on the modulation of intermolecular interactions with poor operability. Therefore, a facile design strategy of UORTP materials, which directly correlates molecular structure with phosphorescence performance, is highly desired.

Based on the above considerations, we proposed a facile strategy for modulating intramolecular hydrogen bonding (IHB) and push–pull electron effects (PPEEs) to construct UORTP luminophores with high Φ_P. We envisaged that molecular planarization can be manipulated by IHB, thus conducive to promoting conjugation and inducing intermolecular π–π interactions. In addition, the intramolecular PPEEs improved by the introduction of heteroatoms and heavy atoms can probably lead to decreased ΔE_{ST} and increased SOC. Meanwhile, the π–π interactions induced by IHBs and PPEEs are expected to promote intermolecular electron coupling, thus obtaining efficient UORTP materials (Scheme 1). To verify our hypothesis, six compounds were designed and synthesized in two series (with and without heavy atoms), namely 9-phenyl-9*H*-carbazole (CzPh), 9-(pyridin-2-yl)-9*H*-carbazole (CzPy), 9-(pyrimidin-2-yl)-9*H*-carbazole (CzPM), 9-(4-bromophenyl)-9*H*-carbazole (CzPhBr), 9-(5-bromopyridin-2-yl)-9*H*-carbazole (CzPyBr), and 9-(5-bromopyrimidin-2-yl)-9*H*-carbazole (CzPMBr). As shown in Fig. 1A, each compound contained a donor group (carbazole) and an acceptor group (phenyl, pyridinyl or pyrimidinyl derivatives). The experimental results demonstrated that IHBs and PPEEs gradually intensified with increasing numbers of nitrogen atoms in the acceptor group. As a result, the molecular structure became planar and intermolecular π–π interactions were remarkably enhanced. In particular, CzPM and CzPMBr with dual IHBs and the strongest PPEEs exhibited the phosphorescence lifetimes (τ_P) of 1.31 s and 233 ms with Φ_P values of 1.7% and 39.7%, respectively. Theoretical calculations revealed that IHB-induced planarization together with PPEEs greatly contributed to the increased SOC. More interestingly, high-lying intersystem crossing (HISC) from excited singlet states (S_m, $m > 1$) to triplet states (T_n, $n > 1$) was found in the compounds CzPM and CzPMBr with strong IHBs and PPEEs, accounting for higher Φ_P values. In short, this work demonstrates that highly efficient UORTP materials can be successfully achieved by structural control of IHBs and PPEEs, promoting the rapid development of UORTP materials.

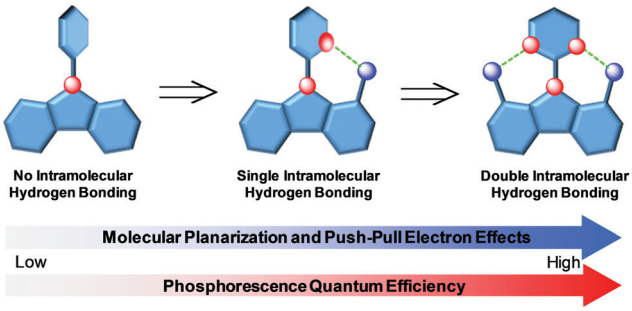

Scheme 1 Illustration of the structural control strategy of IHBs and PPEEs for boosting the efficiency of UORTP materials.

Jianguo Wang

Prof. Jianguo Wang was born in Inner Mongolia (China). He received his PhD in 2014 from the Institute of Chemistry, Chinese Academy of Sciences (ICCAS) under the supervision of Prof. Deqing Zhang. He spent two years as a postdoctoral fellow in Prof. Ben Zhong Tang's group at the Hong Kong University of Science and Technology (HKUST). In 2019, he started his research group as a Professor at Inner Mongolia University. His research interests focus on organic optoelectronic materials with aggregation-induced emission (AIE) features for disease diagnosis and treatment.

Results and discussion

Synthesis and characterization

Six carbazole derivatives were synthesized *via* a one-step reaction in high yields (Schemes S1–S6, ESI†) and characterized by standard spectroscopic methods with satisfactory results (Fig. S1–S18, ESI†). All compounds were purified multiple times by high-performance liquid chromatography and recrystallization (Fig. S19, ESI†). Their single crystals were obtained by slow solvent evaporation of ethyl acetate and characterized crystallographically (Table S1, ESI†).

Photophysical performance

First, the absorption spectra of the obtained six compounds were recorded as shown in Fig. S20 (ESI†). The experimental results showed that they have similar absorption bands. All

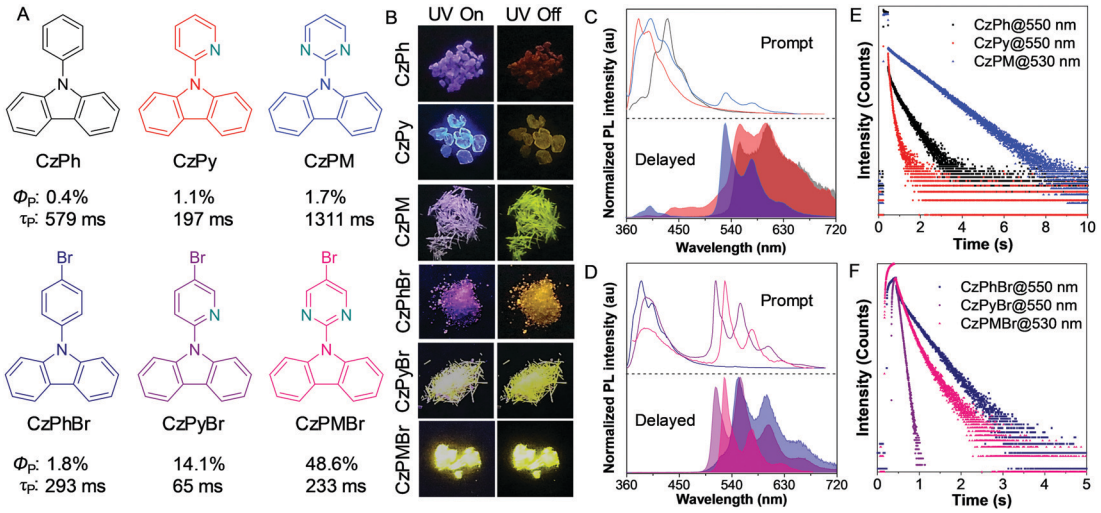

Fig. 1 (A) Chemical structures and phosphorescence properties of CzPh, CzPy, CzPM, CzPhBr, CzPyBr, and CzPMBr in the crystalline state. (B) Photographs of the six crystalline solids taken before (left) and after (right) switching off the 365 nm excitation source. Prompt (unfilled) and delayed (filled) PL spectra (C and D) and time-resolved decay of phosphorescence (E and F) of CzPh (black), CzPy (red), CzPM (blue), CzPhBr (navy), CzPyBr (purple), and CzPMBr (pink) in the crystalline state at 298 K. The delayed PL spectra were taken after a delay of 50 ms. Excitation wavelength: 360 nm.

compounds in the crystalline state exhibited typical RTP characteristics with an afterglow of a few seconds after removing 365 nm excitation (Fig. 1B and Fig. S21, ESI†). Steady-state photoluminescence (PL) spectra were recorded to further investigate their photophysical properties. As shown in Fig. 1C, for CzPh, CzPy and CzPM without heavy atoms, their prompt PL spectra showed a strong fluorescence band at 360–500 nm with lifetimes of 50.54 ns (@430 nm for CzPh), 4.32 ns (@382 nm for CzPy) and 8.6 ns (@400 nm for CzPM) (Fig. S22–S24 and Tables S2–S4, ESI†) at room temperature, respectively. In particular, for CzPM, apart from the dominant high-energy fluorescence band, weak dual emission in the long-wavelength region (500–720 nm) was also captured in its prompt PL spectrum. The delayed PL spectra of the three compounds were found to be very similar at a low-energy region of 500–720 nm (Fig. 1C). The τ_P values were calculated to be 579 ms (@550 nm), 197 ms (@550 nm) and 1.31 s (@530 nm) for CzPh, CzPy and CzPM at room temperature, respectively (Fig. 1A, E and Tables S5–S12, ESI†). Their τ_P was significantly prolonged under vacuum due to isolation from moisture and oxygen (Tables S13–S15, ESI†). These results indicate that CzPh, CzPy and CzPM have UORTP properties. Their absolute Φ_P (integrating sphere method) increases gradually from 0.4% to 1.7% with the addition of nitrogen atoms to the acceptor moiety, which is entirely consistent with our expectation (Fig. 1A). Their variable temperature steady-state and transient PL spectra were recorded (Fig. S25–S33, ESI†). When the temperature was lowered from 298 K to 80 K, the intensity of their phosphorescence signal gradually increased, and their τ_P increased to 966 ms, 808 ms and 1.88 s, respectively (Fig. S25, S28, S31 and Tables S6, S9, S12, ESI†). Additionally, as the temperature decreased, a new phosphorescence band at 488 nm gradually appeared for the three compounds. This implies that at low temperatures, the triplet excitons in T_n may transfer directly to the ground state (S_0) without passing through T_1 *via* internal conversion. Notably, different from CzPh and CzPy, some unique features were observed for CzPM. An emission band at 360–450 nm with a lifetime of 435 ms at 298 K was recorded in the delayed PL spectrum (Fig. 1C and Table S10, ESI†). The emission intensity remarkably enhanced at 340 K, but almost completely disappeared at 240 K (Fig. S31 and S32, ESI†), which can be attributed to triplet–triplet annihilation (TTA).

To confirm the applicability of our design strategy, CzPhBr, CzPyBr and CzPMBr were designed by introducing bromine atoms. As expected, their Φ_P increased to 1.8%, 14.1% and 48.6%, respectively (Fig. 1A), compared to their heavy atom-free counterparts CzPh, CzPy and CzPM. Interestingly, Φ_P was proportional to the number of nitrogen atoms in the acceptor moiety. This indicated that the anticipatory design strategy of UORTP materials is of certain universality. The steady-state PL spectra showed that the three brominated compounds possessed a stronger phosphorescence emission band at 500–720 nm than their counterparts (Fig. 1D). In particular, for CzPyBr and CzPMBr, even in the prompt PL spectrum, there was still a stronger phosphorescence band than the fluorescence band, which can be ascribed to more efficient SOC between the S_m and T_n promoted by the heavy atom effect and PPEE. The τ_P of these brominated compounds is shortened to 293 ms (CzPhBr), 65 ms (CzPyBr) and 233 ms (CzPMBr), respectively (Fig. 1A and F). The brominated compounds also displayed temperature and oxygen dependent phosphorescence behaviours (Fig. S34–S44 and Tables S16–S27, ESI†). Additionally, a new phosphorescence band ($T_n \rightarrow S_0$) at 450–500 nm with τ_P values of 150 ms (@460 nm) for CzPhBr and 60 ms (@470 nm) for CzPyBr appeared and increased gradually, which is similar to that of their heavy atom-free counterparts (Fig. S35, S39 and Tables S17, S21, ESI†).

The phosphorescence spectra of all compounds exhibited excitation wavelength dependence (Fig. S45, ESI†). Time-resolved

emission spectra further showed that CzPy displayed an intense phosphorescence emission band around 450 nm even at room temperature (Fig. S46, ESI†). This may be due to the fact that CzPy has more triplet states lower than S_1. For CzPM, a TTA emission band centered at 400 nm was clearly observed, indicating that TTA could easily occur due to the longest τ_P of 1.31 s and efficient population of T_n states.

Single crystal diffraction analyses

Single crystal X-ray diffraction analyses were carried out to further uncover the origin of enhanced Φ_P. As shown in Fig. 2A, two molecular conformations were observed in the single crystal structures of CzPh and CzPy, while only one conformation was recorded for the other four compounds. For CzPh, the dihedral angles between the carbazole and benzene rings in two conformations were 77.60° and 53.46°, respectively. For CzPy with pyridine as the acceptor moiety, a single hydrogen bond between the carbazole and pyridine rings was found at distances of 2.771 Å and 2.630 Å for each conformation, leading to decreased dihedral angles of 56.93° and 47.20°. When pyrimidine served as the acceptor, CzPM was almost planar with a dihedral angle of 5.87°, accompanied by shorter IHB distances of 2.291 Å and 2.312 Å. Similar tendencies were found in CzPhBr, CzPyBr and CzPMBr. Their dihedral angles between the donor and acceptor were found to be 48.44°, 38.13°, and 4.93°, respectively. IHB interactions were not observed in CzPhBr. For CzPyBr, the distance of the IHB was 2.498 Å, and stronger IHB interactions at 2.316 Å and 2.320 Å were observed for CzPMBr. This elucidated that the molecular conformation was driven to be planar by progressively strengthened IHBs. Since intermolecular packing modes of organic phosphors are directly correlated with their molecular structures and conformations, the intermolecular packing of the six phosphors was further investigated. As depicted in Fig. 2B and Fig. S47, S48 (ESI†), the intermolecular interactions of CzPh and CzPhBr were mainly C–H···π interactions, with the absence of π–π interactions. In addition, dual Br–H interactions between adjacent CzPhBr molecules were also observed. These C–H···π and Br–H interactions efficiently suppressed the non-radiative transition of triplet excitons, which contributed a lot to their phosphorescence behaviours. In the single crystal of CzPy, apart from plentiful C–H···π interactions, weak π–π (3.438 Å) and intermolecular hydrogen bonding (N···H 2.574 Å) interactions were observed (Fig. 2B and Fig. S49, ESI†). Compared to CzPy, stronger dual π–π interactions (3.423 Å and 3.456 Å) rendered the two adjacent CzPyBr molecules in an antiparallelly head-to-tail arrangement in their crystal structures (Fig. 2B), and the two adjacent layers were locked by intermolecular hydrogen bonding (N···H 2.720 Å) and Br···Br interactions (3.304 Å) (Fig. S50, ESI†). We assumed that the antiparallel arrangements coupled with the stronger intermolecular PPEE of CzPyBr dominantly contributed to its layered stacking pattern and needle-like crystal shape. CzPM and CzPMBr with dual IHB interactions and near-planar structure presented parallel head-to-tail arrangements with strong π–π interactions, forming J-aggregates as a result (Fig. 2B and Fig. S51, S52, ESI†). Also, the intermolecular PPEEs between the carbazole and pyrimidine of adjacent molecules may enhance the intermolecular electronic coupling which greatly promoted the ISC rate. Together, the synergistic effect of J-aggregates and intermolecular electronic coupling induced by π–π stacking and intermolecular PPEEs endowed CzPM and CzPMBr with the highest Φ_P in their series. These results again manifested that highly efficient UORTP can be achieved by enhanced IHBs and PPEEs through regulating the planarity and packing mode of molecular structures.

Theoretical calculation

To further reveal the essence of the UORTP design strategy, time-dependent density functional theory (TD-DFT) calculations were performed to investigate the energy level information and SOC matrix elements (ξ) of the six UORTP luminophores. In Fig. S53

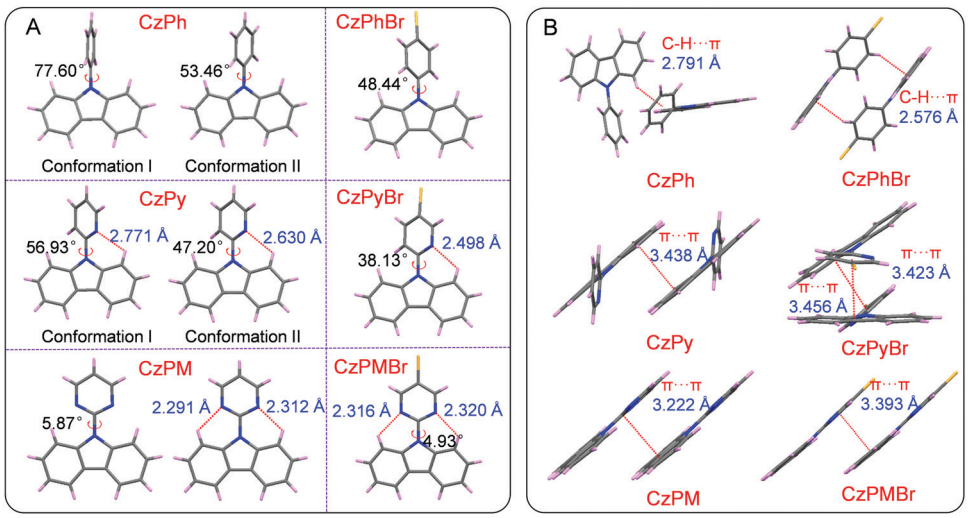

Fig. 2 (A) Single crystal structures, conformations, dihedral angles and intramolecular hydrogen bonding distances of CzPh, CzPy, CzPM, CzPhBr, CzPyBr, and CzPMBr. (B) C–H···π and π–π interactions of CzPh, CzPy, CzPM, CzPhBr, CzPyBr, and CzPMBr.

(ESI†), as the number of nitrogen-atom increased from CzPh to CzPM, the energy gaps between S_1 and S_0 decreased gradually. Three UORTP materials with bromine atoms exhibited the same tendency (Fig. 3A and Fig. S54, ESI†). This is due to the better molecular planarity and conjugation degree resulting from enhanced IHBs and PPEEs. The energy level of the excited state indicated that CzPy possessed more transition pathways from S_1 to T_n than CzPh, accounting for its higher Φ_P (Fig. S53A and S53B, ESI†). Even so, both the compounds showed negligible $\xi(S_m,T_n)$ between S_m and T_n, demonstrating their poor ISC efficiency. Surprisingly, CzPM with higher Φ_P exhibited fewer transition pathways compared to CzPy. In order to find out the reason, the $\xi(S_m,T_n)$ of CzPM was analysed (Fig. S53C, ESI†). The results displayed that its $\xi(S_3,T_7)$ can be up to 1.576 cm^{-1}, and ΔE_{S3T7} is only 0.09 eV. Therefore, HISC may exist in CzPM due to the perturbation of the charge transfer state and the small ΔE_{S3T7}, leading to its higher Φ_P. To verify the occurrence of HISC, the energy levels and ξ values of CzPhBr, CzPyBr and CzPMBr were then calculated. The results further confirmed the HISC pathways with larger ξ values (Fig. 3A and Fig. S54, ESI†). For example, $\xi(S_3,T_7)$ and $\xi(S_3,T_3)$ of CzPMBr are as high as 39.95 cm^{-1} and 6.737 cm^{-1}, respectively. Thus, the dual influences of the heavy atom effect and PPEE on the orbital transition configuration and the charge transfer strength resulted in a more efficient HISC. The calculated natural transition orbitals demonstrated that almost all of the electronic configurations of excited states in CzPh and CzPy are dominated by $\pi \rightarrow \pi^*$ transition (Fig. S55 and S56, ESI†). Hence, a small ξ was observed because the ISC from S_m ($\pi \rightarrow \pi^*$) to T_n ($\pi \rightarrow \pi^*$) is spin-forbidden. In contrast, the S_m involved in the HISC of CzPM and CzPMBr possesses an $n \rightarrow \pi^*$ configuration due to the presence of a heteroatom and heavy atom, while T_n still exhibits a predominant $\pi \rightarrow \pi^*$ configuration (Fig. S57–S60, ESI†). Thus, efficient SOC occurs and the HISC process opens up for the spin-allowed transition from $n \rightarrow \pi^*$ to $\pi \rightarrow \pi^*$. In addition, T_n ($\pi \rightarrow \pi^*$) also guarantees the generation of RTP with long lifetimes. Together, with the aid of IHBs and PPEEs, the efficient HISC breaks through the limitations of the highly efficient RTP caused by the spin-forbidden ISC process.

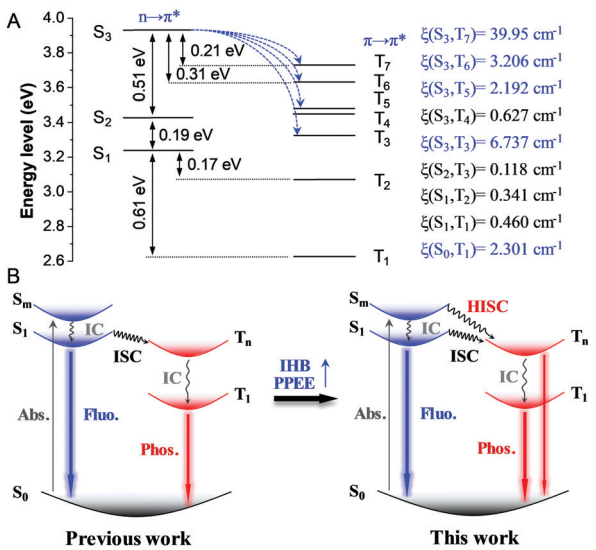

Fig. 3 (A) Schematic diagrams of the TD-DFT calculated energy levels, possible HISC channels and spin–orbit coupling matrix elements of CzPMBr. (B) Proposed mechanism of UORTP produced by the high-lying intersystem crossing between S_m ($m > 1$) and T_n ($n > 1$). (S_0 = ground state, S_1 and S_m = excited singlet state, T_1 and T_n = excited triplet state, Abs. = Absorption, Fluo. = Fluorescence, Phos. = Phosphorescence, ISC = intersystem crossing, IC = internal conversion, HISC = the intersystem crossing between high-lying S_m ($m > 1$) and T_n ($n > 1$), IHB = intramolecular hydrogen bonding, PPEE = push–pull electron effect)

Anti-counterfeiting

Given the superior ultralong RTP properties of CzPMBr, its potential application as a security ink for anti-counterfeiting in calligraphy and painting was investigated. As shown in Fig. 4, a seven-character quatrain and a painting containing fluorescence area and phosphorescence area were made. The quatrain is an acrostic poem that contained four sentences, and the first word of each sentence is composed of the Chinese words "室温磷光", namely, "room temperature phosphorescence". The painting was entitled "Cat and Mouse". The fluorescence areas were written by an aggregation-induced emission luminogen TTAPE-Me dissolved in aqueous solution. In contrast, the phosphorescence areas were drawn by using the THF solution of TPE with 5% of CzPMBr (Fig. S61, ESI†). When exposed to 365 nm UV light, the whole poem was seen with bright blue emission. When turning off UV excitation, however, only yellow-emissive Chinese words "室温磷光" were observed, and it lasted for several seconds benefiting from the ultralong RTP lifetime of CzPMBr. Similarly, a blue-emissive cat emerged in the painting under UV irradiation. Upon switching off the light source, a mouse giving yellow emission appeared instead. These results demonstrated that the UORTP properties of CzPMBr made it a promising candidate for a security ink material for anti-counterfeiting.

Conclusions

In summary, we proposed a facile design strategy based on the structural control of IHBs and PPEEs to construct highly efficient UORTP materials. Accordingly, two series of carbazole derivatives with a D–A structure were designed and synthesized. When the acceptor changed from phenyl, pyridinyl to pyrimidinyl, their molecular conformations became planar with strengthened IHB interactions and PPEEs. This further led to the changes in intermolecular interactions from C–H···π to π–π interactions. The strong π–π interactions combined with intermolecular D–A interactions are in favour of the formation of J-aggregates and intermolecular electron coupling, promoting the ISC rate. Consequently, CzPM and CzPMBr with dual IHBs and the strongest PPEEs exhibited τ_P of 1.31 s and 233 ms and highest Φ_P of 1.7% and 48.6%. Theoretical investigations revealed that the heavy atom effect and PPEE strengthened the intramolecular charge transfer states to change the orbital transition mode of S_m. This makes HISC possible, which plays a crucial role in preparing UORTP materials. Specifically, $\xi(S_3,T_7)$ of CzPMBr reached up to 39.95 cm^{-1}, and thus CzPMBr

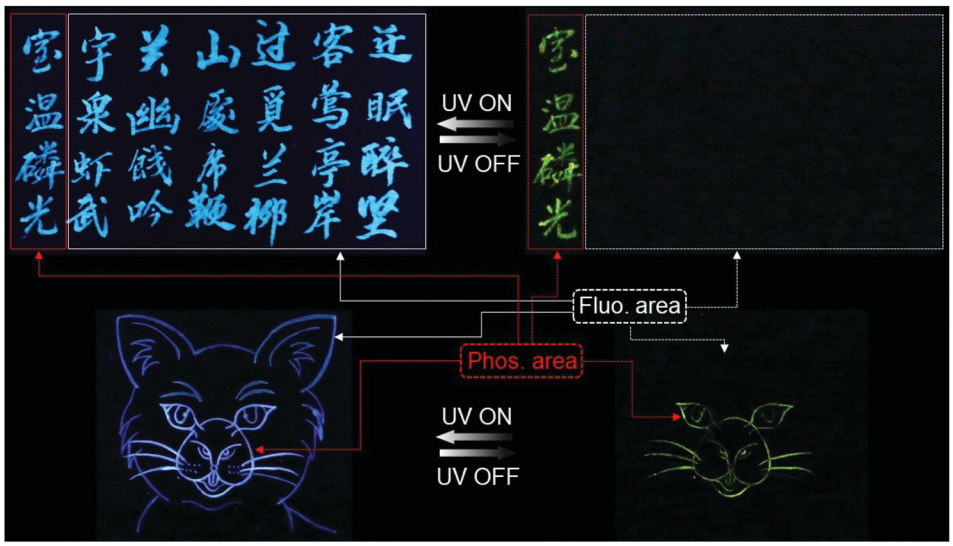

Fig. 4 Photographs of calligraphy and painting under 365 nm irradiation (left) and after removing the excitation light (right).

exhibited the highest Φ_P. Finally, CzPMBr has been successfully used as a multifunctional ink for anti-counterfeiting in calligraphy and painting due to its excellent RTP properties. Collectively, the design strategy based on the structural control of IHBs and PPEEs will greatly widen the design platform of UORTP materials. Meanwhile, the discovery of the HISC process will also provide a new idea for the design of UORTP materials.

Author contributions

Guoyu Jiang: conceptualization, validation, formal analysis, investigation, data curation, methodology, funding acquisition, and writing – original draft, review and editing. Qiyao Li: visualization, formal analysis, and writing – review and editing. Anqi Lv: visualization, investigation, and data curation. Lingxiu Liu: investigation. Jianye Gong: investigation. Huili Ma: investigation, methodology, conceptualization, and writing – review and editing. Jianguo Wang: conceptualization, validation, formal analysis, methodology, funding acquisition, writing – review and editing, and supervision. Ben Zhong Tang: writing – review and editing, and supervision.

Conflicts of interest

There are no conflicts to declare.

Acknowledgements

This work was supported by the National Natural Science Foundation of China (22165020, 22161034, 21871060, and 21973043), the Grassland Talent Program of Inner Mongolia Autonomous Region of China, the Science and Technology Program of Inner Mongolia (2021GG0154), the Natural Science Foundation of Inner Mongolia Autonomous Region of China (2020JQ02 and 2020MS02004), the Natural Science Foundation of Jiangxi Province (20192BCBL23013) and the Young Science and Technology Talents Cultivation Project of Inner Mongolia University (21221505). We also thank Mr Zhenghe Zhai at ORDOS No. 1 High School for the poetry creation, and Mr Meijia Chen and Ms Qingqing Chen at Gannan Normal University for calligraphy and painting. We are grateful to the High Performance Computing Center at Nanjing Tech University for supporting the computational resources.

Notes and references

1 N. A. Kukhta and M. R. Bryce, *Mater. Horiz.*, 2021, **8**, 33–55.
2 Q. Li and Z. Li, *Acc. Chem. Res.*, 2020, **53**, 962–973.
3 B. Zhou, G. Xiao and D. Yan, *Adv. Mater.*, 2021, **33**, e2007571.
4 H. Gao and X. Ma, *Aggregate*, 2021, **2**, e38.
5 K. Liu, K. Huang, A. Lv, W. Ye, Y. Yang, K. Shen, J. Zhi, H. Wang, R. Zhang, J. Wang, H. Ma, H. Shi, W. Yao, Z. An and W. Huang, *Chem. Commun.*, 2021, **57**, 7276–7279.
6 W. Dai, X. Niu, X. Wu, Y. Ren, Y. Zhang, G. Li, H. Su, Y. Lei, J. Xiao, J. Shi, B. Tong, Z. Cai and Y. Dong, *Angew. Chem., Int. Ed.*, 2022, **61**, e202200236.
7 K. Jiang, L. Zhang, J. Lu, C. Xu, C. Cai and H. Lin, *Angew. Chem., Int. Ed.*, 2016, **55**, 7231–7235.
8 X. Yu, H. Zhang and J. Yu, *Aggregate*, 2021, **2**, 20–34.
9 K. Jiang, X. Gao, X. Feng, Y. Wang, Z. Li and H. Lin, *Angew. Chem., Int. Ed.*, 2020, **59**, 1263–1269.
10 Y. Lei, W. Dai, J. Guan, S. Guo, F. Ren, Y. Zhou, J. Shi, B. Tong, Z. Cai, J. Zheng and Y. Dong, *Angew. Chem., Int. Ed.*, 2020, **59**, 16054–16060.
11 M. Jian, Z. Song, X. Chen, J. Zhao, B. Xu and Z. Chi, *Chem. Eng. J.*, 2022, **429**, 132346.
12 Y. Yang, Y. Liang, Y. Zheng, J.-A. Li, S. Wu, H. Zhang, T. Huang, S. Luo, C. Liu, G. Shi, F. Sun, Z. Chi and B. Xu, *Angew. Chem., Int. Ed.*, 2022, DOI: **10.1002/anie.202201820**.

13 Y. Ren, W. Dai, S. Guo, L. Dong, S. Huang, J. Shi, B. Tong, N. Hao, L. Li, Z. Cai and Y. Dong, *J. Am. Chem. Soc.*, 2022, **144**, 1361–1369.
14 L. Ma, S. Sun, B. Ding, X. Ma and H. Tian, *Adv. Funct. Mater.*, 2021, **31**, 2010659.
15 X. Yu, K. Liu, H. Zhang, B. Wang, G. Yang, J. Li and J. Yu, *CCS Chem.*, 2021, **3**, 252–264.
16 Y.-J. Ma, X. Fang, G. Xiao, B. Lu and D. Yan, *Chem. Commun.*, 2021, **57**, 6684–6687.
17 D. Wang, Y. Xie, X. Wu, Y. Lei, Y. Zhou, Z. Cai, M. Liu, H. Wu, X. Huang and Y. Dong, *J. Phys. Chem. Lett.*, 2021, **12**, 1814–1821.
18 H. Wang, Q. Li, J. Zhang, H. Zhang, Y. Shu, Z. Zhao, W. Jiang, L. Du, D. L. Phillips, J. W. Y. Lam, H. H. Y. Sung, I. D. Williams, R. Lu and B. Z. Tang, *J. Am. Chem. Soc.*, 2021, **143**, 9468–9477.
19 R. Gui, H. Jin, Z. Wang, F. Zhang, J. Xia, M. Yang, S. Bi and Y. Xia, *Nanoscale*, 2015, **7**, 8289–8293.
20 X. Zhen, R. Qu, W. Chen, W. Wu and X. Jiang, *Biomater. Sci.*, 2021, **9**, 285–300.
21 W. Wu, C. Zhang, T. W. Rees, X. Liao, X. Yan, Y. Chen, L. Ji and H. Chao, *Anal. Chem.*, 2020, **92**, 6003–6009.
22 Y. Hou, G. Jiang, J. Gong, R. Sha and J. Wang, *Chem. Res. Chin. Univ.*, 2021, **37**, 73–82.
23 Z. He, H. Gao, S. Zhang, S. Zheng, Y. Wang, Z. Zhao, D. Ding, B. Yang, Y. Zhang and W. Z. Yuan, *Adv. Mater.*, 2019, **31**, 1807222.
24 H.-B. Cheng, Y. Li, B. Z. Tang and J. Yoon, *Chem. Soc. Rev.*, 2020, **49**, 21–31.
25 Y. Wang, H. Gao, J. Yang, M. Fang, D. Ding, B. Z. Tang and Z. Li, *Adv. Mater.*, 2021, **33**, 2007811.
26 J. Qi, H. Ou, Q. Liu and D. Ding, *Aggregate*, 2021, **2**, 95–113.
27 H.-J. Yu, Q. Zhou, X. Dai, F.-F. Shen, Y.-M. Zhang, X. Xu and Y. Liu, *J. Am. Chem. Soc.*, 2021, **143**, 13887–13894.
28 F. Lin, H. Wang, Y. Cao, R. Yu, G. Liang, H. Huang, Y. Mu, Z. Yang and Z. Chi, *Adv. Mater.*, 2022, **34**(15), 2108333.
29 W. Zhao, Z. Z. THe, W. Y. L. Jacky, Q. Peng, H. Ma, Z. Shuai, G. Bai, J. Hao and Z. T. Ben, *Chem*, 2016, **1**, 592–602.
30 L. Gu, X. Wang, M. Singh, H. Shi, H. Ma, Z. An and W. Huang, *J. Phys. Chem. Lett.*, 2020, **11**, 6191–6200.
31 L. Gu, H. Wu, H. Ma, W. Ye, W. Jia, H. Wang, H. Chen, N. Zhang, D. Wang, C. Qian, Z. An, W. Huang and Y. Zhao, *Nat. Commun.*, 2020, **11**, 944.
32 Q. Huang, Z. Lin and D. Yan, *Small Struct.*, 2021, **2**, 2100044.
33 X. Cai, X. Li, G. Xie, Z. He, K. Gao, K. Liu, D. Chen, Y. Cao and S.-J. Su, *Chem. Sci.*, 2016, **7**, 4264–4275.
34 H. Ma, A. Lv, L. Fu, S. Wang, Z. An, H. Shi and W. Huang, *Ann. Phys.*, 2019, **531**, 1800482.
35 L. Feng, C. Li, L. Liu, Z. Wang, Z. Chen, J. Yu, W. Ji, G. Jiang, P. Zhang, J. Wang and B. Z. Tang, *ACS Nano*, 2022, **16**, 4162–4174.
36 Z. Chen, F. Ni, Z. Wu, Y. Hou, C. Zhong, M. Huang, G. Xie, D. Ma and C. Yang, *J. Phys. Chem. Lett.*, 2019, **10**, 2669–2675.
37 H. Gao, B. Ding, C. Wang and X. Ma, *J. Mater. Chem. C*, 2021, **9**, 16581–16586.
38 H. Li, H. Li, J. Gu, F. He, H. Peng, Y. Tao, D. Tian, Q. Yang, P. Li, C. Zheng, W. Huang and R. Chen, *Chem. Sci.*, 2021, **12**, 3580–3586.
39 J. Ren, Y. Wang, Y. Tian, Z. Liu, X. Xiao, J. Yang, M. Fang and Z. Li, *Angew. Chem., Int. Ed.*, 2021, **60**, 12335–12340.
40 L. Yang, X. Wang, G. Zhang, X. Chen, G. Zhang and J. Jiang, *Nanoscale*, 2016, **8**, 17422–17426.
41 J. Wang, X. Gu, H. Ma, Q. Peng, X. Huang, X. Zheng, S. H. P. Sung, G. Shan, J. W. Y. Lam, Z. Shuai and B. Z. Tang, *Nat. Commun.*, 2018, **9**, 2963.
42 X. Sun, B. Zhang, X. Li, C. O. Trindle and G. Zhang, *J. Phys. Chem. A*, 2016, **120**, 5791–5797.
43 Z. Yang, Z. Mao, X. Zhang, D. Ou, Y. Mu, Y. Zhang, C. Zhao, S. Liu, Z. Chi, J. Xu, Y.-C. Wu, P.-Y. Lu, A. Lien and M. R. Bryce, *Angew. Chem., Int. Ed.*, 2016, **55**, 2181–2185.
44 O. Bolton, K. Lee, H.-J. Kim, K. Y. Lin and J. Kim, *Nat. Chem.*, 2011, **3**, 205–210.
45 Y. Xiong, Z. Zhao, W. Zhao, H. Ma, Q. Peng, Z. He, X. Zhang, Y. Chen, X. He, J. W. Y. Lam and B. Z. Tang, *Angew. Chem., Int. Ed.*, 2018, **57**, 7997–8001.
46 X. Sun, X. Wang, X. Li, J. Ge, Q. Zhang, J. Jiang and G. Zhang, *Macromol. Rapid Commun.*, 2015, **36**, 298–303.
47 J. Yang, M. Fang and Z. Li, *Aggregate*, 2020, **1**, 6–18.
48 H. Wu, C. Hang, X. Li, L. Yin, M. Zhu, J. Zhang, Y. Zhou, H. Ågren, Q. Zhang and L. Zhu, *Chem. Commun.*, 2017, **53**, 2661–2664.
49 Z.-A. Yan, X. Lin, S. Sun, X. Ma and H. Tian, *Angew. Chem., Int. Ed.*, 2021, **60**, 19735–19739.
50 B. Wu, N. Guo, X. Xu, Y. Xing, K. Shi, W. Fang and G. Wang, *Adv. Opt. Mater.*, 2020, **8**, 2001192.
51 D. Li, J. Yang, M. Fang, B. Z. Tang and Z. Li, *Sci. Adv.*, 2022, **8**, eabl8392.
52 B. Ding, H. Gao, C. Wang and X. Ma, *Chem. Commun.*, 2021, **57**, 3154–3157.
53 B. Chen, W. Huang, X. Nie, F. Liao, H. Miao, X. Zhang and G. Zhang, *Angew. Chem., Int. Ed.*, 2021, **60**, 16970–16973.
54 J. Zhang, S. Xu, Z. Wang, P. Xue, W. Wang, L. Zhang, Y. Shi, W. Huang and R. Chen, *Angew. Chem., Int. Ed.*, 2021, **60**, 17094–17101.
55 X. Liu, W. Dai, J. Qian, Y. Lei, M. Liu, Z. Cai, X. Huang, H. Wu and Y. Dong, *J. Mater. Chem. C*, 2021, **9**, 3391–3395.
56 Y. Lei, J. Yang, W. Dai, Y. Lan, J. Yang, X. Zheng, J. Shi, B. Tong, Z. Cai and Y. Dong, *Chem. Sci.*, 2021, **12**, 6518–6525.
57 X. Zhang, L. Du, W. Zhao, Z. Zhao, Y. Xiong, X. He, P. F. Gao, P. Alam, C. Wang, Z. Li, J. Leng, J. Liu, C. Zhou, J. W. Y. Lam, D. L. Phillips, G. Zhang and B. Z. Tang, *Nat. Commun.*, 2019, **10**, 5161.
58 S. Hirata, K. Totani, J. Zhang, T. Yamashita, H. Kaji, S. R. Marder, T. Watanabe and C. Adachi, *Adv. Funct. Mater.*, 2013, **23**, 3386–3397.
59 Z. An, C. Zheng, Y. Tao, R. Chen, H. Shi, T. Chen, Z. Wang, H. Li, R. Deng, X. Liu and W. Huang, *Nat. Mater.*, 2015, **14**, 685–690.
60 Z. Yin, M. Gu, H. Ma, X. Jiang, J. Zhi, Y. Wang, H. Yang, W. Zhu and Z. An, *Angew. Chem., Int. Ed.*, 2021, **60**, 2058–2063.
61 W. Ye, H. Ma, H. Shi, H. Wang, A. Lv, L. Bian, M. Zhang, C. Ma, K. Ling, M. Gu, Y. Mao, X. Yao, C. Gao, K. Shen,

W. Jia, J. Zhi, S. Cai, Z. Song, J. Li, Y. Zhang, S. Lu, K. Liu, C. Dong, Q. Wang, Y. Zhou, W. Yao, Y. Zhang, H. Zhang, Z. Zhang, X. Hang, Z. An, X. Liu and W. Huang, *Nat. Mater.*, 2021, **20**, 1539–1544.

62 M. Huo, X.-Y. Dai and Y. Liu, *Angew. Chem., Int. Ed.*, 2021, **60**, 27171–27177.

63 X.-K. Ma, W. Zhang, Z. Liu, H. Zhang, B. Zhang and Y. Liu, *Adv. Mater.*, 2021, **33**, 2007476.